In-plane impact behavior of honeycomb structures filled with linearly arranged inclusions

Hiroaki Nakamoto[1], Tadaharu Adachi[*1], Wakako Araki[2]

[1]*Department of Mechanical Sciences and Engineering, Tokyo Institute of Technology, 2-12-1 Ookayama, Meguro-ku, Tokyo 152-8552, Japan*

[2]*Department of Mechanical Engineering, Saitama University, 255 Shimo-Okubo, Sakura-ku, Saitama City, Saitama 338-8570, Japan*

* Corresponding author
Tadaharu Adachi
Associate Professor
E-mail: adachi@mech.titech.ac.jp
Department of Mechanical Sciences and Engineering
Tokyo Institute of Technology
2-12-1 O-okayama, Meguro-ku, Tokyo 152-8552, Japan
Phone: +81-3-5734-2156
Fax: +81-3-5734-2893

Abstract

Honeycomb structures filled with linearly arranged inclusions were analyzed with a finite element method (FEM) to study how the arrangement of rigid inclusions affects the in-plane impact behavior of honeycomb structures. Each model was divided into several cell regions by inclusion lines. The analysis revealed the effect of inclusion lines on the mean stress of the cell region, maximum displacement of the cell region, and the order of deformed cell regions. Maximum displacement of the cell region was proportional to the width of the cell region, and mean stress of the cell region decreased as the width of the cell region increased. Approximate equations for the maximum displacement and mean stress of the cell region were derived. The approximations accounted for the deformation process of the honeycomb models with inclusion lines and revealed the dependence of the order of the deformed cell region on the mean stress of the regions. The validity of the approximate equations was confirmed by comparing them with experimental results. It was found that the approximate equations enabled us to design the in-plane impact behavior of honeycomb structures filled with linearly arranged inclusions.

Key words: Honeycomb structure; Energy absorption; Finite element method; In-plane impact behavior; Inclusions

1. Introduction

The honeycomb is a typical cellular structure. Honeycomb structures composed of metals, polymers, ceramics, and paper are commonly used as energy absorbing materials for various engineering applications such as packaging and protective materials, core materials of sandwich panels, and building materials. Deformations of honeycombs have been analyzed by assuming that the honeycombs are composed of an infinite repetition of identical unit cells [1-10].

Recently, honeycomb structures having geometrical irregularities such as non-periodic cells, imperfect cells and locally strengthened cells have been investigated. Non-periodic honeycomb models are often created by using Voronoi tessellations [11]. The elastic constants of Voronoi honeycombs were found to vary by several percent compared with regular ones [12]. Zhu et al. [13] developed Voronoi models using periodic boundary conditions. Zheng et al. [14] studied the deformation mode of Voronoi models undergoing dynamic crushing. Gan et al. [15] analyzed three-dimensional Voronoi models. Recently, Hwang et al. [16] suggested a laminate model to analyze foam materials having non-uniform cell sizes due to the manufacturing process. Imperfect cells in honeycomb structures were found to decrease the stiffness and strength of a honeycomb [17, 18]. Silva and Gibson [19] showed the

effect of imperfect cells on Voronoi honeycombs. Local strengthening of honeycomb structures was analyzed by using a honeycomb structure filling some cells with stiff inclusions [23]. Various structural irregularities such as irregular shapes, non-uniform cell wall thicknesses [20], wavy cell walls, non-uniform wall thickness, missing cell walls, non-periodic cells [21], clustered inclusions, and holes [22] were analyzed.

In our previous study [24], the in-plane impact behavior of honeycomb structures randomly filled with rigid inclusions was analyzed by using a finite element method (FEM) to clarify effect of inclusions on the deformation process and energy absorption. It was found that inclusions disturbed the deformation process. Collapsed cells were shielded and pinned by inclusions. Percolation of inclusions was observed; the deformation of the honeycomb ceased when inclusions connected the impact side and fixed side of the model. Mean stress increased and densification strain, namely, the maximum deformation of the honeycomb model decreased as the volume fraction of inclusions increased. The results indicated the possibility of improving and designing the energy absorption characteristics of honeycomb structures through proper arrangement of inclusions.

In this study, to explore the possibility of designing the in-plane impact behavior of honeycomb structures, we clarified the effect of linearly arranged inclusions

filling honeycomb structures by using FEM and obtained useful equations for designing the energy absorption characteristics of such structures. The validity of the equations derived from FE analysis was confirmed by comparing them with the experimental results. The effect of linearly arranged inclusions on the in-plane impact behavior of the honeycomb structures was elucidated.

2. Analysis

2.1 Analytical model

2.1.1 Unit cell

Analytical models were two-dimensional honeycomb structures composed of equilateral hexagonal cells, as shown in Fig. 1 (a), in which every side length of the unit cell was l and the depth was the unit length. Because actual honeycomb structures are manufactured by expanding a stack of partially bonded thin plates [7], the thickness of cell walls in the Y-direction was $2h$, while that of the other walls was h, as shown in Fig. 1 (b).

2.1.2 Analytical models

The model was composed of M rows (the number of unit cells in the Y-direction) and N columns (the number of unit cells in the X-direction). The horizontal and vertical lengths of the model were $W\ (=(1+3N)/2)$ and $L\ (=\sqrt{3}Ml)$, respectively.

The rigid inclusions were all parallel to the *Y*-direction; namely, they were linearly arranged.

Each model was divided into several cell regions by the inclusion lines. The width of the cell region between inclusion lines, namely, the interval of the lines was defined as the number of cells between inclusions, *n* in Fig. 1 (b). Honeycomb models with geometries as listed in Table 1 were analyzed to consider the effect of these inclusions on the model's deformation behavior.

2.2 Analytical conditions

The honeycomb models of the finite element analysis are compressed with a low-velocity impact. Every honeycomb model was fixed on the right side, and a rigid impactor having a mass of 5.0 kg collided with the left side of the model with an impact velocity of 1 m/s, as shown in Fig. 2. The impact loading was only due to the collision with the rigid impactor. The width of the impactor was much larger than those of the honeycomb models. The apparent cross-sectional area of models were the same as *W*.

This problem was analyzed as a plane-stress problem by using an FEM with an explicit time integration (RADIOSS, version 4.4q). Each cell wall was discretized by three two-dimensional Euler beam elements without transverse shearing deformation, and the material was assumed to be elasto-perfectly plastic. The inclusions were

approximated as rigid bodies. The friction constant was assumed to be zero. Contact deformation between the honeycomb model and the rigid impactor was analyzed using the penalty method.

Compressive stress, σ, was defined as the reaction force of the impactor divided by the apparent cross-sectional area of the undeformed honeycomb model, *W*. The displacement of the honeycomb model on the impact side, *u*, was evaluated from the displacement of the impactor after collision.

3. Numerical results

To clarify the effect of inclusion lines on the in-plane impact behavior of the honeycombs, models with the material properties and geometries listed in Table 2 were analyzed.

3.1 Deformation process

Fig. 3 shows the deformation process of the model without inclusions, L0(20). First, cells collapsed in oblique directions; namely, shear bands occurred and grew from the corners of the impact side of the honeycomb (Fig. 3 (b)). More shear bands occurred (Fig. 3 (c)), and the model became completely densified (Fig. 3 (d)).

Figs. 4 and 5 show the deformation processes of models with inclusion lines, L2(6) and L6(2). At first, the cell region between the impact side and inclusion line

became densificated as shown in Figs. 4 (b) and 5 (b). After that, cell regions between inclusion lines deformed (Figs. 4 (c) and 5 (c)); the regions deformed from one neighbor to another on the impact side. Each cell region crushed individually, because of the shielding effect of the inclusion lines. Finally, region between fixed side and inclusion line deformed (Figs. 4 (d) and 5 (d)). The honeycomb models completely densified when the impact side and fixed side became connected by inclusions; namely, percolation of inclusions occurred.

3.2 Stress-displacement curve

Fig. 6 shows the compressive stress-displacement curves of models L2(6) and L6(2). The results for the model without inclusions, L0(20), is plotted as a reference. The curve of L0(20) had a stress plateau caused by shear band growth after the elastic range with an initial sharp peak. At the end of the plateau (the shear band could not grow), the stress peaked because compressive deformation of cells began in triangle regions near the fixed side of the honeycomb. Finally, the model became densified at u = 148.0 mm. The curves of the models with inclusion lines fluctuated with several stress peaks caused by densification of each cell region, and mean stresses were higher than the one for the model without inclusions. The mean stress increased as the width of the cell region became narrower (decreasing n). The curve of model L2(6) had two peaks at

u = 33.9 mm and 67.4 mm until the densification of the whole honeycomb. The curve for model L6(2) had six peaks, at u = 8.39, 16.7, 29.1, 41.3, 53.1 and 63.1 mm. The mean stress due to the deformations between the peaks depended on the width of the cell region and were larger than the one of the model without inclusions.

4. Discussion

4.1 Maximum displacement

Let us consider the maximum displacement, $u_{\max}$, for each cell region, i.e., the displacement, at a local densification within a cell region. $u_{\max}$ can be normalized by dividing it by the side length of the unit cell, l. Fig. 7 shows the relationship between normalized maximum displacement, $u_{\max}/l$, and the width of the region, n. The maximum displacements of the cell regions between impact boundary and the inclusion line, between the inclusion lines, and between the inclusion line and the fixed boundary were distinctly plotted by considering the effect of boundary conditions; the impacted boundary where cells can freely deform in the *Y*-direction, the boundary on the line inclusions and the fixed boundary where deformation of cells in *Y*-direction is restricted. The boundary conditions of the cell regions are abbreviated as follows; between impact side and inclusion line (IL), between inclusion lines (LL), and between the inclusion line and fixed side (LF). The maximum displacements depended on the boundary

conditions of the cell regions. LF had the largest maximum displacement, and LL had the lowest. $u_{\max}/l$ was proportional to n in all cases and could expressed by the following approximate equations fitted by the least-squares method:

$$\frac{u_{\max}}{l} = \begin{cases} 1.29n & \text{(IL)} \\ 1.39n & \text{(LL)} \\ 1.46n & \text{(LF).} \end{cases} \quad (1)$$

4.2 Mean stress

Next, let us consider the mean stress in each cell region, σ_M. σ_M can be normalized by dividing it by the plastic collapse stress of a honeycomb made of elasto-plastic materials, σ_{pl} [24], as given by [25]:

$$\sigma_{pl} = \frac{2}{3}\left(\frac{h}{l}\right)^2 \sigma_{ys}. \quad (2)$$

Fig. 8 shows the relationship between normalized mean stress of the cell region, σ_M/σ_{pl}, and the width of the region, *n*, of cells in IL, LL, and LF. The mean stresses depended on the boundary conditions of the cell regions. The mean stress of cells in LF was the highest and lowest in IL. σ_M/σ_{pl} decreased as *n* increased and can be approximated by the following power laws:

$$\frac{\sigma_M}{\sigma_{pl}} = \begin{cases} 1.41n^{-0.37} & \text{(IL)} \\ 1.69n^{-0.42} & \text{(LL)} \\ 1.65n^{-0.22} & \text{(LF).} \end{cases} \quad (3)$$

4.3 Order of cell region deformation

Now let us discuss the order of cell region deformation of models with inclusion lines. Compression of the equal-interval model deforms the cell region from the impact side to the fixed side. The order of cell region deformation is in ascending order of mean stress as shown in Fig. 8.

5. Comparison with experimental results

5.1 Procedure

We confirmed the validity of the mean stress-displacement response of a honeycomb structure with several inclusion lines by using the mean stress and maximum displacement of cell regions gotten from the unit cell geometry and material properties (Eqs. (1) and (3)). In the experiment, models L0(18), L2(8/6/4) and L3(7/4/3/2) where chosen as honeycomb specimens. The specimens were composed of 0.076 mm thick aluminum alloy sheets (A3003H19). The geometry and material properties listed in Table 3; model L2(8/6/4) had 2 inclusions lines and 3 cell regions of n = 8, 6, 4. Model L3(7/4/3/2) had 3 inclusions lines and 4 cell regions of n = 7, 4, 3, 2. Acrylic resin (Struers, Versocit) was filled into some cells of the specimens to act as inclusions.

We manufactured an experimental apparatus for applying an axial impact to a specimen and measuring the impact force and deformation of the specimen as shown in

Fig. 9. The apparatus was a falling drop weight testing machine. Fig. 9 (a) shows the impactor (10.5 kg), which was made of a steel bar 1000 mm long and 48 mm in diameter. The impactor was freely dropped on a cross-head on a specimen. The impact velocity measured in a preliminary experiment was ninety percent of the theoretical value, $\sqrt{2gH}$, where H and g are the drop height of the impactor and the gravity acceleration. The drop height was constant (about 150 mm); namely, impact speed was about 1.5 m/s. A rubber plate was set on the cross-head to prevent repeated impacts due to rebounding of the impactor. Sandpaper was set under the specimen to keep it in place. The deformation process was recorded by using a high-speed video camera (Shimadzu, HPV-1). The displacement of the steel cross-head was measured as the deformation of a specimen, u, by using an optical displacement transducer (Zimmer, 100B). The impact force history, P, was also measured using a load cell made of steel. The details of the load cell are shown in Fig. 9 (b). The lowest natural frequency of this load cell was 7 kHz, as determined in a preliminary experiment [26]. From the axial deformation histories of the top end of a specimen and impact force P, the absorbed energy, E_{ab}, defined as the external work of the impactor, was calculated as follows;

$$E_{ab} = \int P(u)du. \qquad (4)$$

5.2 Experimental results and discussion

5.2.1 Results for model L2(10/6/2)

Table 4 shows mean stress, maximum deformation, and the order of deformation of each cell region in model L2(10/6/2) derived from the prediction equation. In the Table, deformation of the cell regions was predicted to occur in order of lower mean stress given by Eq. (3). The predicted order of the deformed cell region matched the experimental result in Fig. 10.

Fig. 11 shows the stress-displacement curves of model L2 (10/6/2) measured in the experiment and the predicted mean stress-displacement curve given by Eqs (2) and (3). The predicted curve was drawn by using $u_{\max}$ and σ_M for each cell region listed in Table 4. The stress-displacement curve of model L0(18) measured in the experiment is plotted as a reference. The experimental stress-displacement curve initially showed compressive stress due to collapse of cell region IL having n = 10. After that, compressive stress increased through collapse of cell region LL having n = 6, and the model eventually completely densified. The experimental result was in good agreement with the predicted mean stress-displcement curve. Additionally, the experiment confirmed that the plateau stress in the curves of model L2(10/6/2) was higher than that of model L0(18).

Fig. 12 shows the relationship between absorbed energy per unit volume of the

honeycomb structures, E_{ab}, and displacement for model L2(10/6/2). The absorbed energy of the experimental results was calculated with Eq. (4) and the predicted energies were calculated by dividing the area below the mean stress-displacement curve in Fig. 11 by *L*. The predictions result agreed with the experimental results. The absorbed energy of model L2(10/6/2) was confirmed to be higher than the that of model L0(18).

5.2.1 Results for model L3(7/4/3/2)

Table 5 shows mean stress, maximum deformation and the order of deformation of each cell region in model L3 (7/4/3/2) derived from Eqs. (2) and (3).

Fig. 13 shows the experimental stress-displacement curve of model L3(7/4/3/2) and the predicted mean stress-displacement curve. The predicted curve was drawn by using $u_{\max}$ and σ_M of each cell region listed in Table 5. The experimental stress-displacement curve initially showed compressive stress due to collapse of cell region IL having n = 7. After that, compressive stress increased through collapse of cell regions LL having n = 4 and 3, and the model eventually completely densified. The experimental results matched with the predicted mean stress-displcement curve. Fig. 14 shows the relationship between the absorbed energy per unit volume, E_{ab}, and displacement for model L3 (7/4/3/2). The predicted result, which agreed with the

experimental result was larger than the that of model L0(18).

The predicted effect of linearly arranged inclusions derived from FEM analysis was confirmed by comparing it with experimental results. The method using Eqs. (1) and (3) and the order of deformed cell regions in terms of σ_M is an efficient way to predict the compressive stress-displacement curve and energy absorption process of a honeycomb structure having linearly arranged inclusions. A honeycomb structure having a particular energy absorption process; deformation process, compressive stress in the plateau region and absorbed energy, can be designed by using Eqs. (1) and (3) by arranging line inclusions at certain intervals.

6. Conclusion

The in-plane impact behavior of honeycomb structures with linearly arranged inclusions was analyzed by using FEM. On the basis of the FEM results, approximate equations of the mean stress and maximum displacement of the cell region and a method of determining the order of the deformed cell region were devised. The arrangement of line inclusions was discussed as it relates to the design of the deformation process, compressive stress, and absorbed energy of honeycomb structures.

It was found that the maximum displacements of the cell region depended on the boundary conditions of the cell regions; the maximum displacement of the cell

region between the inclusion line and the fixed side was the highest, and the one between the impact side and the inclusion line was the lowest. Each maximum displacement was proportional to the width of the cell region and could be approximated by Eq. (1). The mean stresses of the cell region also depended on the boundary conditions of the cell regions; the mean stress of the cell region between the inclusion line and fixed side was the highest, and the one between the impact side and inclusion line was the lowest. Each mean stress decreased as the width of the cell region increased and could be approximated by Eq. (3). The order of deformation of the cell regions could be determined by comparing the regions' mean stresses.

The validity of the approximate equations was confirmed by comparing them with experimental results. The results indicated that it is possible to design an arbitrary deformation process, compressive stress in the plateau region, and absorbed energy of honeycomb structures by using the approximate equation to arrange line inclusions at certain intervals.

References

[1] Gibson LJ, Ashby MF. Cellular solids: structure and properties, 2nd ed. Cambridge: Cambridge University Press, 1997:93-147.

[2] Ohno N, Okumura D, Noguchi H. Microscopic symmetric bifurcation condition of

cellular solids based on a homogenization theory of finite deformation. J Mech Phys Solids 2002;50:1125-53.

[3] Okumura D, Ohno N, Noguchi H. Elastplastic microscopic bifurcation and post-bifurcation behavior of periodic cellular solids. J Mech Phys Solids 2004;52:641-66.

[4] Jagla EA. The buckling transiton of two-dimensional elastic honeycombs: numerical simulation and Landau theory. J Phys 2004;16:4419-28.

[5] Karagiozova D, Yu TX. Plastic deformation modes of regular hexagonal honeycombs under in-plane biaxial compression. Int J Mech Sci 2004;46:1489-515.

[6] Ruan D, Lu G, Wang B, Yu TX. In-plane dynamic crushing of honeycombs –a finite element study. Int J Impact Eng 2003;28:161-82.

[7] Papka SD, Kyriakides S. In-plane compressive response and crushing of honeycomb. Int J Mech Phys Solids 1994;42:1499-532.

[8] Papka SD, Kyriakides S. Experiments and full-scale numerical simulations of In-plane crushing of a honeycomb. Acta Mater 1998;46:2765-76.

[9] Hönig A, Stronge WJ. In-plane dynamic crushing of honeycomb. Part I: crush band initiation and wave trapping. Int J Mech Sci 2002;44:1665-96.

[10] Hönig A, Stronge WJ. In-plane dynamic crushing of honeycomb. Part II: application to impact. Int J Mech Sci 2002;44:1697-714.

[11] Zhu HX, Thorpe SM, Windle AH. The geometrical properties of irregular two-dimensional Voronoi tessellations. Philos Mag A 2001;12:2765-83.

[12] Silva MJ, Hayes WC, Gibson LJ. The effects of non-periodic microstructure on the elastic properties of two-dimensional cellular solids. Int J Mech Sci 1995;37:1161-77.

[13] Zhu HX, Thorpe SM, Windle AH. The effect of cell irregularity on the high strain compression of 2D Voronoi honeycomb. Int J Solids Struct 2006;46:1061-78.

[14] Zheng Z, Yu J, Li J. Dynamic crushing of 2D cellular structures: A finite element study. Int J Impact Eng 2005;32:650-64.

[15] Gan YX, Chen C, Shen YP. Three-dimensional modeling of the mechanical property of linearly elastic open cell foams. Int J Solids Struct 2005;42:6628-42.

[16] Hwang J-J, Adachi T, Kuwabara T, Araki W. Laminate model expressing mechanical properties of polypropylene foams having non-uniform cell-shape distributions. Mater Sci and Eng A 2008;487:369-76.

[17] Wang A, McDowell DL. Effects of defects on in-plane properties of periodic metal honeycombs. Int J Mech Sci 2003;45:1799-813.

[18] Albuquerque JM, Vaz M Fatima, Fortes MA. Effect of missing walls on the compression behavior of honeycombs. Scripta Mater 1999;41:167-74.

[19] Silva MJ, Gibson LJ. The effect of non-periodic microstructure and defects on the compressive strength of two-dimensional cellular solids. Int J Mech Sci 1997;39:549-63.

[20] Li K, Gao XL, Wang J. Dynamic crushing behavior of honeycomb structures with irregular cell shapes and non-uniform cell wall thickness. Int J Solids Struct 2007;44:5003-26.

[21] Chen C, Lu TJ, Fleck NA. Effect of imperfections on the yielding of two-dimensional foams. J Mech Phys Solids 1999;47:2235-72.

[22] Chen C, Lu TJ, Fleck NA. Effect of inclusions and holes on the stiffness and strength of honeycombs. Int J Mech Sci 2001;43:487-504.

[23] Prakash O, Bichebois P, Brechet Y, Louchet F, Embury JD. A note on the deformation behavior of two-dimensional model cellular structures. Philos Mag A 1996;73:739-51.

[24] Nakamoto H, Adachi T, Araki W. In-plane impact behavior of honeycomb structures randomly filled with rigid inclusions. Int J Impact Eng (in press). doi:10.1016/j.ijimpeng.2008.04.004

[25] Gibson LJ, Ashby MF, Schajer GS, Robertson CI. Mechanics of two-dimensional cellular materials. Proc R Soc London Ser A 1982;382:25-42

[26] Ujihashi S, Sogo T, Matsumoto H, Adachi T. Energy absorption ability of thin-walled members by crushing under impact loading. J Soc Mater Sci Jpn 1993;42:1427-31.

Captions of tables and figures

Table 1 Geometries of honeycomb models

Table 2 Material properties and geometry of unit cell

Table 3 Material properties and geometry of specimens

Table 4 Mean stress, maximum deformation and order of deformed cell region for each cell region of model L2(10/6/2) derived from prediction equation

Table 5 Mean stress, maximum deformation and order of deformed cell region for each cell region of model L3(7/4/3/2) derived from prediction equation

Fig. 1 Analytical model: (a) hexagonal unit cell and (b) honeycomb model with linearly arranged inclusions.

Fig. 2 Analysis conditions.

Fig. 3 Deformation process in model without inclusions, L0(20).

Fig. 4 Deformation process in model L2(6).

Table 1 Geometries of honeycomb models

Model ID	Number of inclusion lines	Width of cell regions *n* (cells)	Number of cells	
			M (cells)	*N* (cells)
L0(20)	0	20	20	21
L1(9)	1	9/9	20	21
L2(6)	2	6/6/6	20	21
L2(16)	2	16/16/16	50	21
L3(4)	3	4/4/4	20	21
L4(3)	4	3/3/3/3	20	21
L6(2)	6	2/2/2/2/2/2	20	21
L9(1)	9	1/1/1/1/1/1/1/1/1	20	21

In the model ID column, the number after L and the ones in the parenthesis denote the number of inclusion lines and widths of cell regions, respectively. As for the widths of cell regions, components of the model are expressed by the widths of the cell regions, *n* and inclusion lines (expressed as slashes).

Table 2 Material properties and geometry of unit cell

Young's modulus (GPa)	70
Poisson's ratio	0.33
Density (kg/m^3)	2700
Yield stress, σ_{ys} (MPa)	34
Side length, l (mm)	5.00
Wall thickness, h (mm)	0.10

Table 3 Material properties and geometry of specimens

Material properties	Young's modulus (GPa)	70		
	Poisson's ratio	0.33		
	Density (kg/m^3)	2700		
	Yield stress, σ_{ys} (MPa)	230		
Unit cell	Side length, l (mm)	4.0		
	Wall thickness, h (mm)	0.076		
Honeycomb	Model ID	L0(18)	L2(10/6/2)	L3(7/4/3/2)
	Number of inclusion lines	0	2	3
	Width of cell regions, n	18	10/6/2	7/4/3/2
	Number of cells	about 18 × 20 (about 351 cells)		

Table 4 Mean stress, maximum deformation and order of deformed cell region for each cell region of model L2(10/6/2) derived from prediction equation

Width of deformed cell region, n	Boundary condition	Mean stress, σ_M (kPa) (Eq. (3))	Maximum deformation, $u_{\max}$ (mm) (Eq. (1))	Order of deformed region (Prediction)
10	IL	33.0	48	1
6	LL	43.3	33.4	2
2	LF	78.4	11.7	3

Table 5 Mean stress, maximum deformation and order of deformed cell region for each cell region of model L3(7/4/3/2) derived from prediction equation

Width of deformed cell region, n	Boundary condition	Mean stress, σ_M (kPa) (Eq. (3))	Maximum deformation, $u_{\max}$ (mm) (Eq. (1))	Order of deformed region (Prediction)
7	IL	38.6	33.6	1
4	LL	51.5	22.2	2
3	LL	58.3	16.7	3
2	LF	78.4	11.7	4

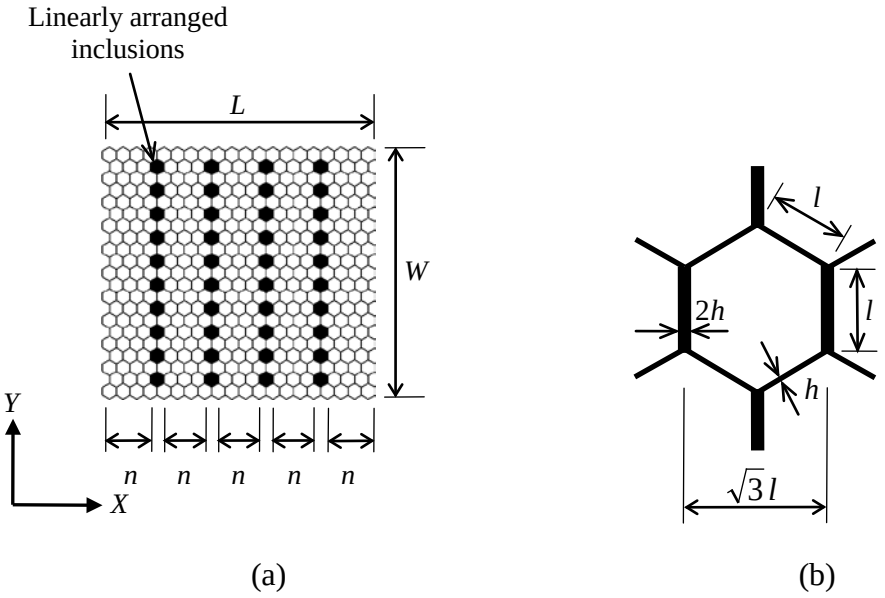

Fig. 1 Analytical model: (a) hexagonal unit cell and (b) honeycomb model with linearly arranged inclusions.

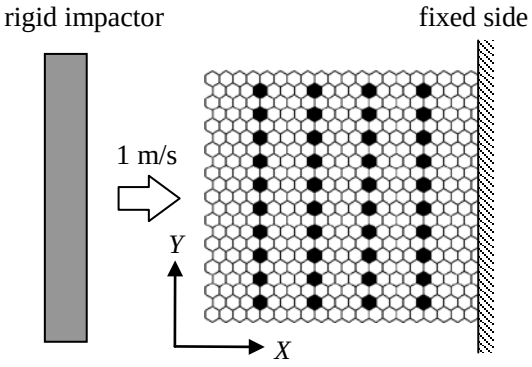

Fig. 2 Analysis conditions.

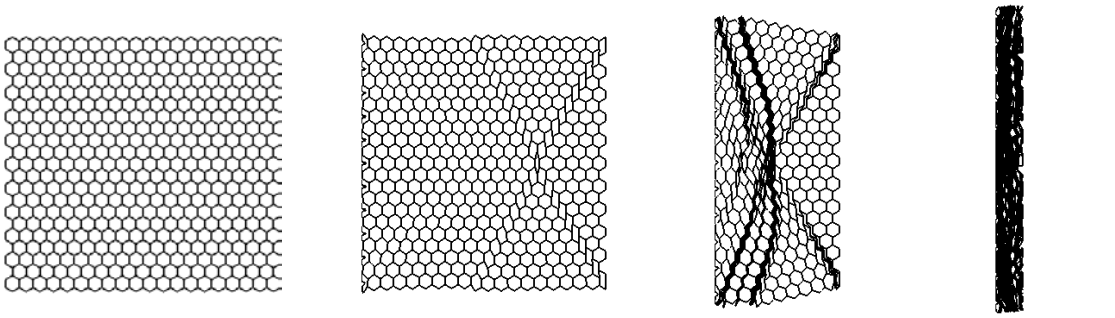

$u = 0$ mm $u = 14.8$ mm $u = 93.0$ mm $u = 148.0$ mm

(a) (b) (c) (d)

Fig. 3 Deformation process in model without inclusions, L0(20).

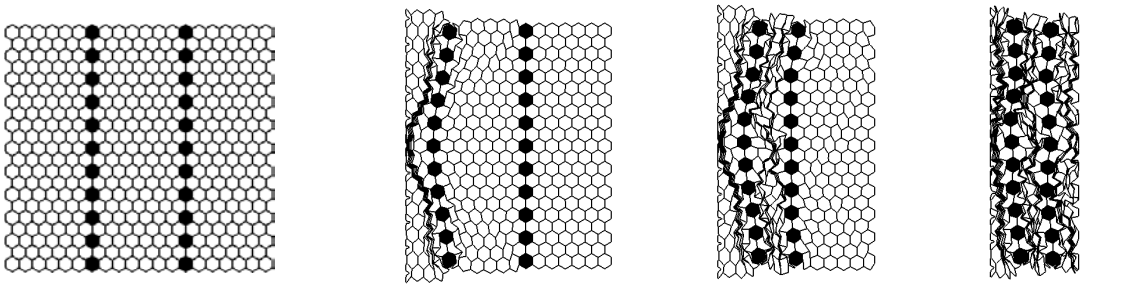

$u = 0$ mm $u = 33.9$ mm $u = 67.4$ mm $u = 114.2$ mm

(a) (b) (c) (d)

Fig. 4 Deformation process in model L2(6).

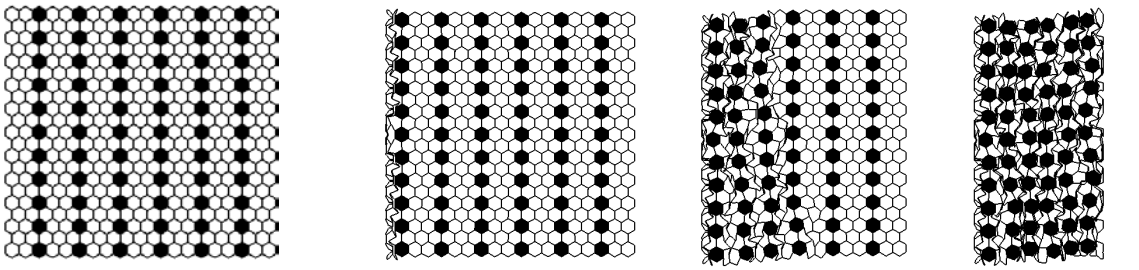

$u = 0$ mm $u = 8.39$ mm $u = 41.3$ mm $u = 87.6$ mm

(a) (b) (c) (d)

Fig. 5 Deformation process in model L6(2).

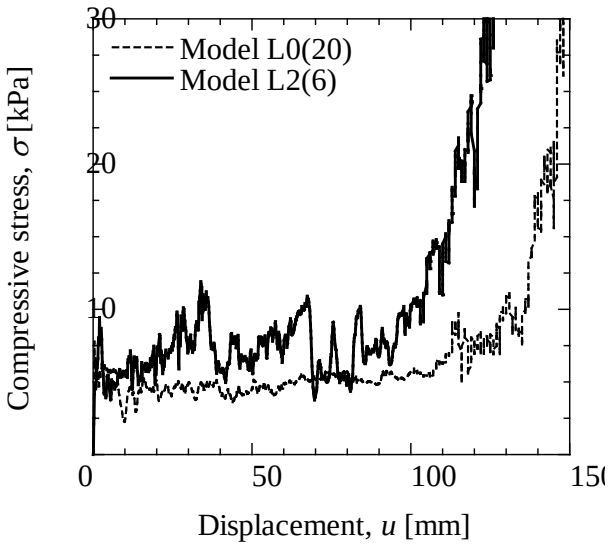

(a)

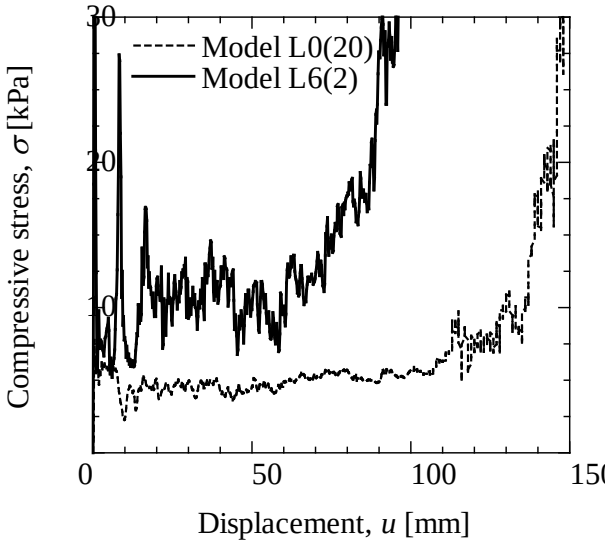

(b)

Fig. 6 Stress-displacement curves of equal-interval models: (a) model L2(6) and (b) model L6(2).

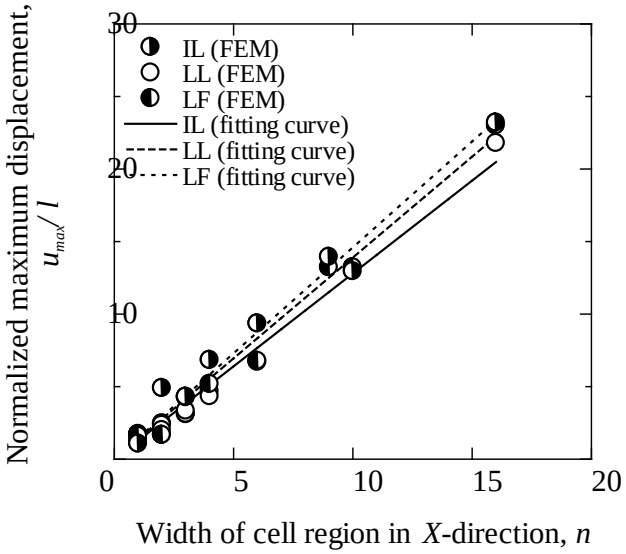

Fig. 7 Relationship between normalized maximum displacement and width of cell region.

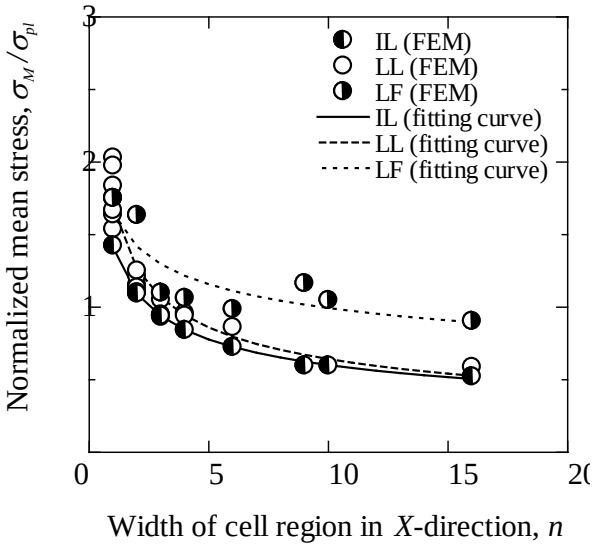

Fig. 8 Relationship between normalized mean stress and width of cell region.

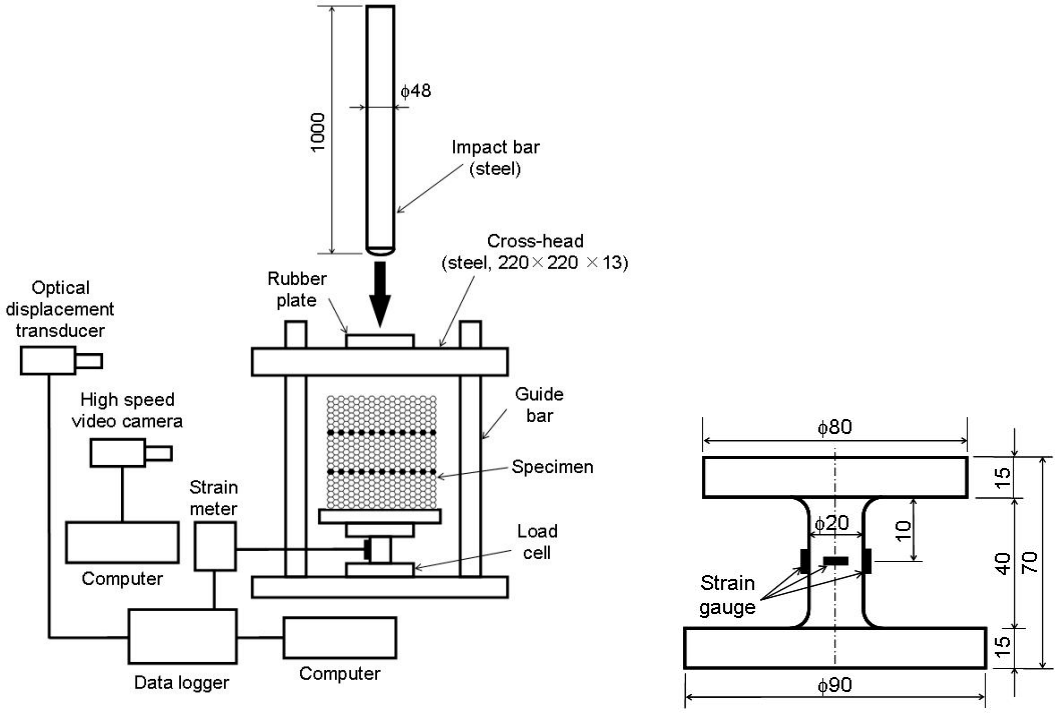

(a) (b)

Fig. 9 Experimental equipment: (a) experimental apparatus and (b) load cell (unit mm).

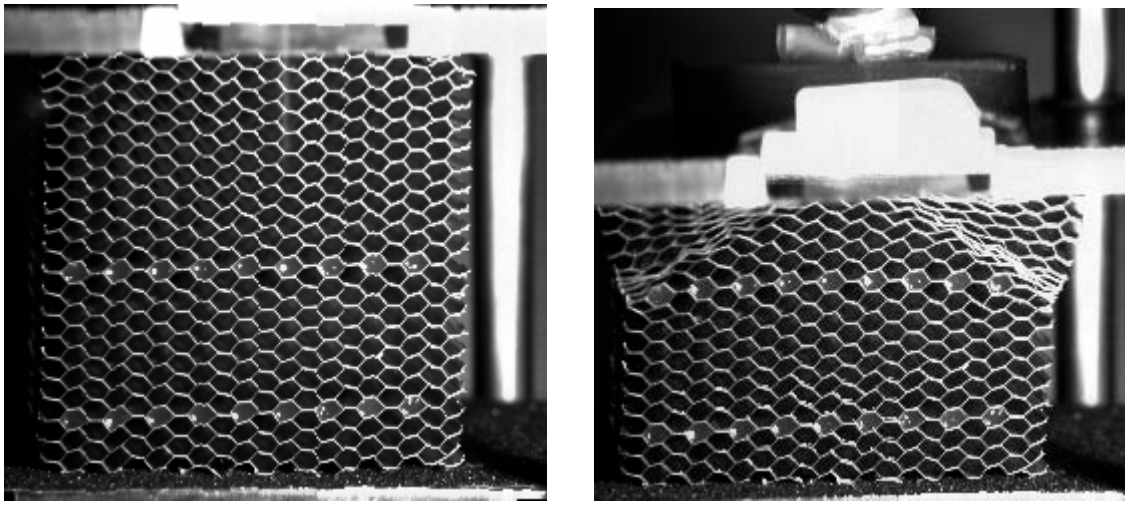

(a) (b)

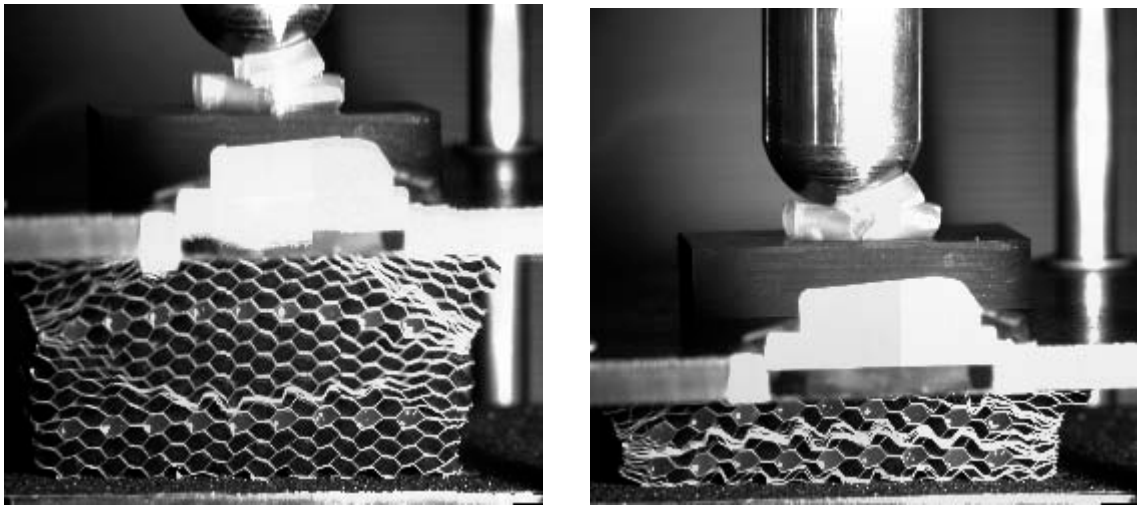

(c) (d)

Fig. 10 Deformation process of model L2(10/6/2) (experimental result).

Impact was applied to the top.

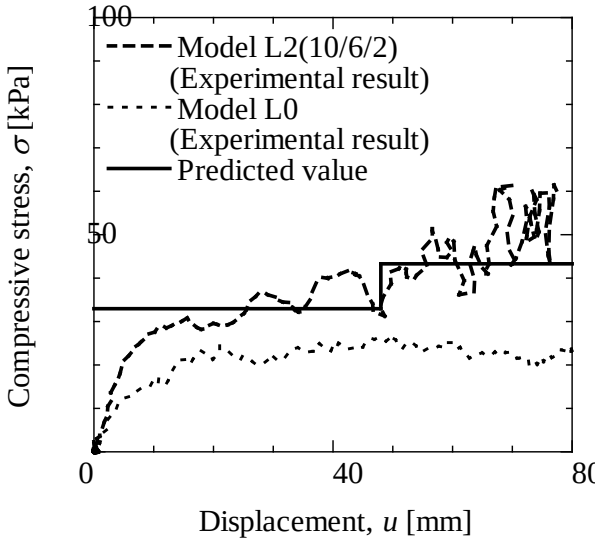

Fig. 11 Stress-displacement curve of model L2(10/6/2).

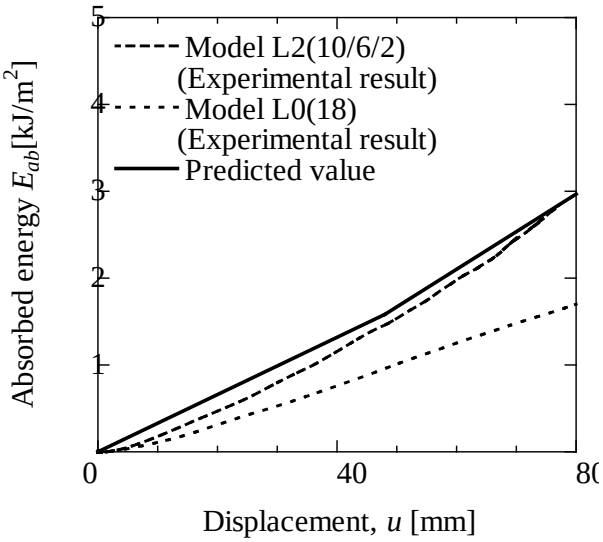

Fig. 12 Absorbed energy per unit volume-displacement curve of model L2(10/6/2).

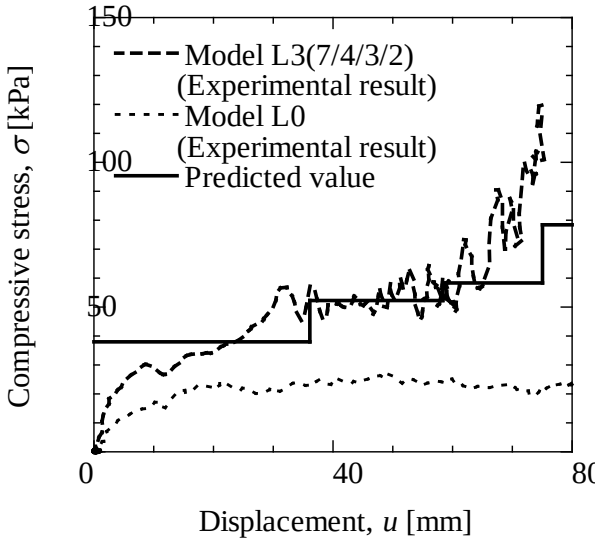

Fig. 13 Stress-displacement curve of model L3(7/4/2).

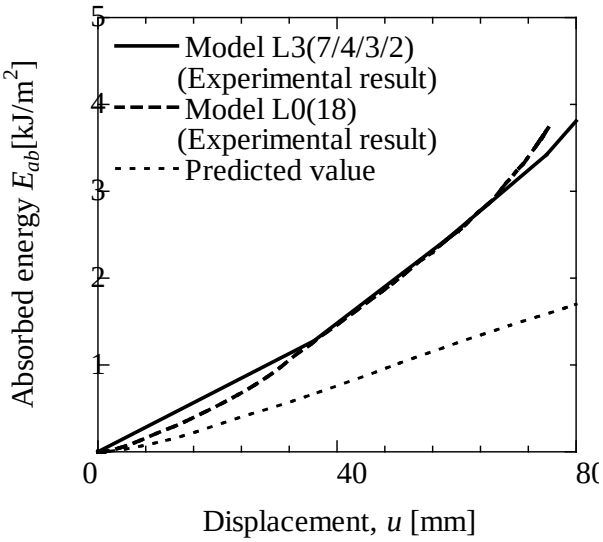

Fig. 14 Absorbed energy per unit volume-displacement curve of model L3(7/4/3/2).